Adsorption (2024) 30:1493–1504
https://doi.org/10.1007/s10450-024-00516-0

Selective Co and Sn co-doped black phosphorene for hydrogen storage: first-principles insights

Abdelazim M. Mebed[1] · **Muhammad Mushtaq**[2] · **Majed Alshamary**[1] · **Meshal Alzaid**[1] · **Amel Laref**[3] · **Alaa M. Abd-Elnaiem**[4]

Received: 9 May 2024 / Revised: 21 June 2024 / Accepted: 24 June 2024 / Published online: 16 July 2024

Abstract

In this study, long-range van der Waals (vdW) and effective Coulomb interaction (U_{eff}) corrected density functional theory (DFT + vdW + U_{eff}) calculations were performed to explore the effect of co-doping (of Co and Sn) on the crystal structure, electronic, magnetic and chemical (H_2 adsorption) properties of phosphorene. The stability of the doped structures was determined with formation energy (E_f) and molecular dynamics (MD) simulations. The dopants were found to form strong bonds with phosphorus (P) atoms. The introduction of Co/Sn-atoms slightly altered the local geometry of phosphorene, resulting in new electronic characteristics. For instance, unlike pristine phosphorene (P_{48}), the co-doped phosphorene ($P_{45}Co_xSn_y$) can exhibit ferrimagnetic (FIM) or ferromagnetic (FM) coupling in the ground state. The doped structures exhibit integral magnetic moments, mainly contributed by the Co-atoms. The $P_{45}Co_1Sn_2$ and $P_{45}Co_2Sn_1$ structures show metallic band structure, while $P_{45}Co_3$ becomes a small band gap (E_g) semiconductor (E_g =0.2 eV). The adsorption of the H_2 molecules was investigated at various sites on un-doped and co-doped phosphorene. It was found that H_2 molecule is weakly adsorbed on un-doped phosphorene, whereas moderate adsorption was observed for co-doped systems. The adsorption energy (E_a) was found to be -0.03, -0.35, -0.48, and − 0.65 eV, respectively for P_{48}, $P_{45}Co_1Sn_2$, and $P_{45}Co_2Sn_1$ and $P_{45}Co_3$. The DOS plots confirmed that the observed adsorption is due to the s-d interaction between H-atom and the doped Co-atom. The Bader charge and charge density difference (CDD) analysis showed that H_2 molecule acts as a charge acceptor and doped phosphorene as a charge donor. In addition, the effect of strain on adsorption was also considered. The adsorption capacity of the doped systems decreased with the number of H_2 molecules. These findings show that co-doped phosphorene can be used for spin-based nanodevices and hydrogen capture for energy storage applications.

Keywords Phosphorene · First-principles · Co-doping · Hydrogen storage

1 Introduction

Hydrogen, being the most abundant, high energy content, and eco-friendly fuel, has been highlighted as an alternative fuel that can substitute the climate-changing fossil fuels [1]. Therefore, various techniques are being proposed for the efficient and economical production, storage, and utilization of hydrogen [2]. Currently, hydrogen storage involves either liquefication or compression, which is not suitable for large-scale production. To achieve high storage density, various materials are proposed [3]. In this perspective, due to high specific surface area and low density, two-dimensional (2D) materials are preferred [4–7].

Graphene, also known as the first ultra-thin two-dimensional (2D) material, composed of a honeycomb monolayer lattice of carbon atoms, isolated from graphite in 2004,

✉ Abdelazim M. Mebed
amali@ju.edu.sa

[1] Department of Physics, College of Science, Jouf University, P.O. Box 2014, Al-Jouf, Sakaka, Saudi Arabia

[2] Department of Physics, University of Poonch Rawalakot, Rawalakot 12350, Pakistan

[3] Department of Physics and Astronomy, College of Science, King Saud University, Riyadh, Saudi Arabia

[4] Physics Department, Faculty of Science, Assuit University, Assuit 71516, Egypt

exhibits unique electronic, transport, and mechanical properties, has opened new horizons in the field of nanoelectronics [8, 9]. Owing to its technical scope, the scientists and researchers devoted great efforts to exploring other 2D materials. So far some well-known 2D materials including silicene [10], germanene [11], boron-nitride [12], metal dichalcogenides [13], and metal carbides/nitrides [14–17], etc., have been realized with a rich diversity in electronic, transport and chemical properties [18, 19].

The group-IV elements (phosphorus P, arsenic As, antimony Sb, and bismuth Bi), commonly known as pnictogens have layered structure in bulk form, where individual layers are stacked by weak van-der-Waals (vdW) interactions. Such a layered structure provides the opportunity for the exfoliation of individual layers. Depending on the crystal lattice, phosphorus can have three allotropes namely white-phosphorus (WP), red-phosphorus (RP), and black-phosphorus (BP). The 2D sheet of PB, called phosphorene was first obtained in 2014 from the bulk orthorhombic crystal in the mechanical exfoliation method and demonstrated to have high carrier mobility and an on-off ratio of 10^4, highly suitable for field-effect-transistor (FET) applications [20]. The monolayer of PB has a puckered structure formed by the P-atoms and exhibits semiconducting properties with a direct band gap (E_g) of 1.5 eV [21]. Later on, in 2015, monolayer 2D crystals of As (arsenene) and Sb (antimonene) were simultaneously predicted as indirect bandgap semiconductors with E_g of 2.49 and 2.28 eV, respectively, which can be turned into direct band gap with tensile strain [22]. Antimonene nanosheets were experimentally obtained with vdW epitaxy method [23], while, arsenene sheets were synthesized on Ag(111) substrate [24].

Apart from synthesis, substantial experimental and theoretical efforts have been carried out to explore various aspects of 2D pnictogens [25, 26]. Being non-magnetic in nature, these systems cannot be directly implemented in ultra-thin spintronic devices. Therefore, to induce moment, various strategies have been employed. For instance, non-magnetic phosphorene turned into magnetic on the adsorption of transition metal atoms (Fe, Co, or Ni) [27]. It was found that the presence of vacancy defects can significantly reduce the thermal conductivity and mechanical strength of phosphorene [28]. It was reported that multiple vacancy defects such as Stone-Waals defects are more like to be formed in phosphorene structure due to its large surface area [29]. Previously, it was reported that the H_2 molecule is weakly adsorbed on pristine phosphorene with adsorption energy (E_a) of -0.18 eV [30], thus the material in pristine form cannot be used for hydrogen capture. The Co-decorated phosphorene showed E_a of -0.88 eV and Sn-decorated has E_a of -0.02 eV [31]. In this work, we introduce the co-doping of cobalt (Co) and strontium (Sn) atoms for tuning the adsorption strength of H_2 on phosphorene. Our results showed that the combination of Co and Sn doping can effectively enhance the adsorption strength of phosphorene toward H_2 capture.

2 Computational methods and detail

In this study, spin-polarized first-principles calculations based on density functional theory (DFT) were performed with the Vienna Ab-initio Simulation Package (VASP) [32]. The exchange-correlation part of the total energy was approximated in generalized gradient approximation (GGA) of Perdew-Burke-Ernzerhof (PBE) formalism [33]. The unit-cell geometry of the pristine monolayer puckered phosphorene (ML-P) was fully relaxed (for atomic positions and lattice vectors) with $20 \times 18 \times 1$ k-points, and its band structure was calculated. From the relaxed unit-cell geometry, a $4 \times 3 \times 1$ supercell composed of 48 P-atoms was built and relaxed with $5 \times 5 \times 1$ k-points, and the density of states was computed with $6 \times 6 \times 1$ k-points. The system of ML-P with tri-doping was created by removing three P-atoms in the middle of the supercell and subjected to relaxation with the same k-points used in ML-P. A vacuum space of 20 Å was introduced along the direction normal to the surface of the doped system. The critical energy difference between consecutive iterations was set at 10^{-4} eV and the plane waves were expanded with an energy cut-off of 500 eV. As the long-range vdW forces have a significant effect on adsorption interaction, we have introduced vdW corrections in the calculations. In addition, the Co-3d states are treated with DFT + U_{eff} method where effective Coulomb interaction U_{eff}=U-J, U is Hubbard Coulomb interaction and J is Hund exchange interaction [34]. A U_{eff} of 3.42 eV for Co-3d states has been adopted here per the literature [35].

3 Results and discussion

3.1 Pristine phosphorene

Before exploring the effect of tri-doping, the ground state geometric and electronic band structure of pristine monolayer phosphorene (ML-P) in unit-cell is calculated, shown in Fig. 1(a, b), where unit-cell is marked by blue dotted lines. In the relaxed state, the unit-cell lattice constant along x-direction *a* is 3.298 Å, and the lattice constant in y-direction *b* is 4.619 Å, which are similar to the a = 3.29 Å and b = 4.54 Å reported elsewhere [27]. Unlike the flat structure of graphene, due to sp^3 hybridization, phosphorene has a puckered structure composed of two atomic planes, where each P-atom is connected to three adjacent P-atoms in

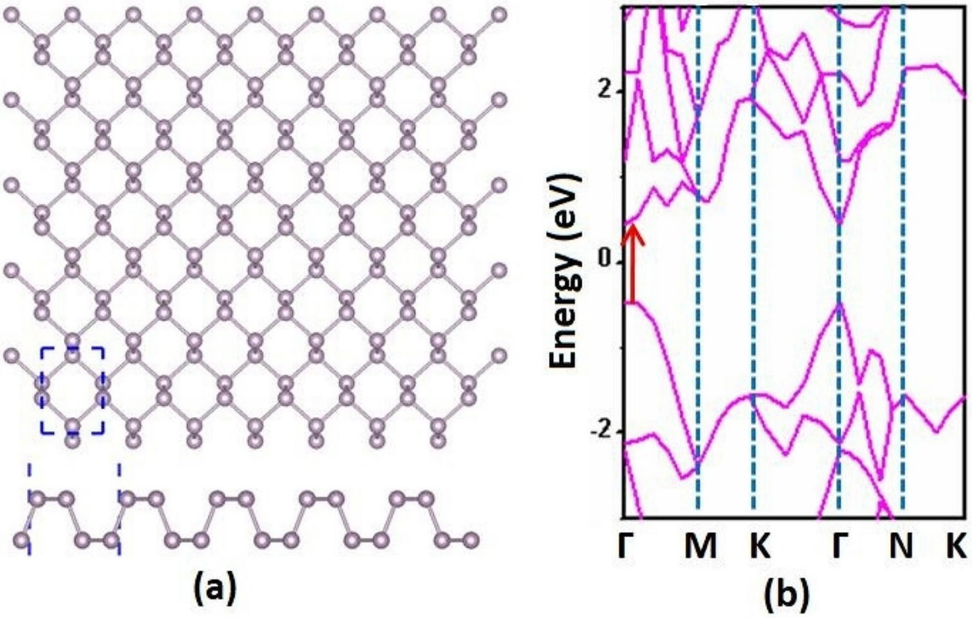

Fig. 1 (**a**) Relaxed geometry (in the top and side views) of monolayer pristine black phosphorene (p-BP) in unit-cell, (**b**) the electronic band structure of p-BP

covalent bonding. In particular, the P-atoms have two types of bond lengths, the shorter bond length is along the zig-zag direction and the longer bond length is along the arm-chair direction. The calculated short and long bond lengths are 2.22 Å and 2.25 Å, respectively. The P-P-P bond angle Φ_P is 95.2 and 104.1 °. The side view of the structure shows that, unlike graphene, ML-P is not a flat one-atom thick, rather it has a puckered structure due to sp^3 hybridization and the thickness of the system is 2.12 Å. Figure 1(b) demonstrates ML-P to be a semiconductor where the valence band and conduction band edge are located at a high symmetric gamma point in the Brillouin zone, giving rise to a direct E_g of 0.91 eV, which is in agreement with the E_g value of 0.957 eV in literature [36].

3.2 Co and Sn co-doped phosphorene (TD-P)

3.2.1 Geometries of co-doped phosphorene

The co-doped structures are obtained by replacing three P-atoms with Co/Sn-atoms. In this way, three selective systems can be achieved: (A) $P_{45}Co_1Sn_2$ (model-A), three P-atoms are replaced by one Co-atoms and two Sn-atom, (B) $P_{45}Co_2Sn_1$ (model-B), three P-atoms are replaced by two Co-atoms and one Sn-atom, (C) $P_{45}Co_3$ (model-C), three P-atoms are replaced by two Co-atoms. Due to the presence of magnetic Co-atom in each model, the geometries are relaxed within spin-polarized calculations to achieve the lowest DFT total energy (E_0). The relaxed geometries are shown in Fig. 2. To provide a better comparison, the relaxed structure of un-doped phosphorene (P_{48}) is also shown in Fig. 1(a). In model-A (Fig. 2b), the top view of the structure shows that doped atoms are slightly displaced from the actual position, causing a stretching in bond lengths. The calculated Co-Sn bond length d_{Co-Sn} is 3.01 Å, greater than the initial value of 2.21 Å, and P-Co bond length d_{P-Co} is 2.27 Å, close to the P-P bond length d_{P-P} of 2.26 Å. However, the two Sn-atoms are also moved closer and have a separation distance of 3.08 Å, shorter than the original value of 3.29 Å. The P-Sn bond length d_{P-Sn} is 2.67 Å. is According to the side view, the doped Co/Sn atoms have significant out-of-place displacements. Such displacements can deform the local geometry, as estimated from the change in bond lengths. In Fig. 2c, one can find that the doped structure has some obvious distortions owing to the formation of new bonds and doped atoms being occupied at new positions. The obtained Co-Sn bond length d_{Co-Sn} is 2.74 Å and 2.67 Å. Likewise, d_{Co-Co} is 2.64 Å, d_{P-Co} is 2.31 Å, and d_{P-Sn} is 2.62 Å. Although bond lengths at doping sites are somewhat changed, the doped atoms are not moved out of the plane. In model-C, each doped Co-atom forms bonds with neighboring P- and Co-atoms. The value of d_{P-Co}, d_{Co-Co} is 2.25 Å, d_{P-Co} is 2.48 Å.

3.3 Stability

The stability of the designed structures is determined via formation energy calculated by equation (a) [37–39].

$$E_f = E_{doped-phosporene} + 3\mu_P - x\mu_{Co} - y\mu_{Sn} - E_{phosporene} \quad (1)$$

where $E_{doped-phosporene}$ is the DFT total energy of Co/Sn-doped phosphorene, $\mu_P, \mu_{Co}, \mu_{Sn}$ represent the chemical

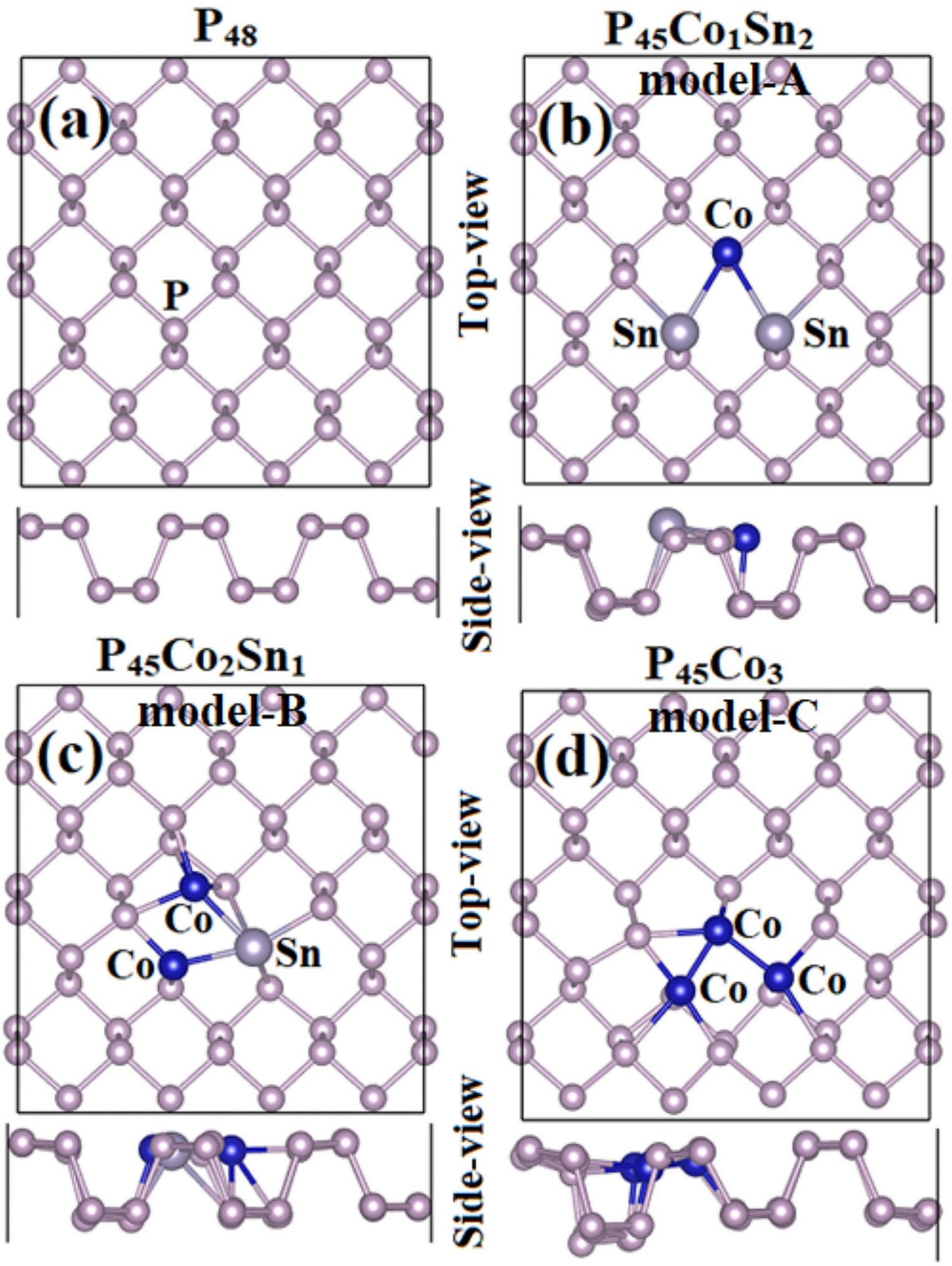

Fig. 2 Relaxed geometries of (**a**) pristine black phosphorene (P_{48}), (**b**) one Co and two Sn doped phosphorene ($P_{45}Co_1Sn_2$), (**c**) two Co and one Sn doped phosphorene ($P_{45}Co_2Sn_1$), (**d**) three Co-doped phosphorene ($P_{45}Co_3$)

potential of P, Co, and Sn, $E_{phosporene}$ is the DFT total energy of un-doped phosphorene, $x\,(y)$ is the number of Co (Sn) atoms doped. The chemical potential of P is taken as the total energy of un-doped phosphorene per atom, whereas the chemical potential of Co/Sn is simply the energy of a single isolated atom. The calculated per-doped atom E_f is -3.05, -3.15, and −2.81 eV/atom. These values of formation energy are within the range of formation energy (-0.4 to -3.2 eV) reported for dual-doped graphene [38].

To further evaluate the structural stability molecular dynamics (MD) simulations are conducted for 5 ps in the NVT ensemble (T = 300 K). The variation in total energy E_0 is monitored over time, shown in Fig. 3. It is noticed that E_0 does not show large fluctuations over time, which means that the structure does not undergo the breaking of chemical bonds or reconstruction. Thus, the present systems are assumed to be stable and could be synthesizable.

3.4 Magnetic and electronic properties

To explore the magnetic properties, the ground state magnetic coupling, the total magnetic moment per supercell (M), and atomic magnetic moment (m) (listed in Table 1) are calculated. As mentioned above, having no unpaired electrons,

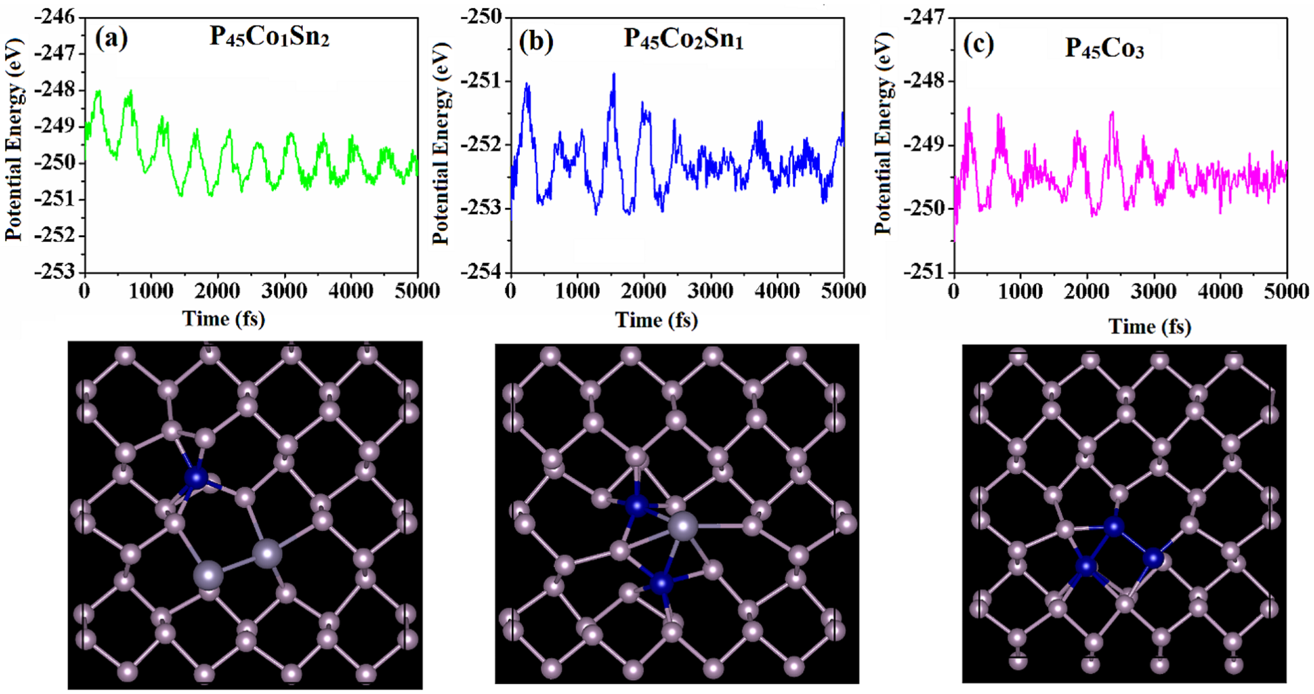

(d) $P_{45}Co_1Sn_2$ at T=300 K (e) $P_{45}Co_2Sn_1$ at T=300 K (f) $P_{45}Co_3$ at T=300 K

Fig. 3 Variation in potential energy with MD time for (**a**) $P_{45}Co_1Sn_2$, (**b**) $P_{45}Co_2Sn_1$), (**c**) $P_{45}Co_3$. The corresponding structures at temperature (T) of 300 K after 5000 fs are shown in lower panels in (**d**), (**e**) and (**f**).

Table 1 Adsorption energy E_a (eV), charge transfer from adsorbent to adsorbate ΔQ|e|, vertical distance between adsorbent and adsorbate h (Å), minimum distance d (Å), H-H bond length d_{H-H}, Fermi energy E_F (eV), the total magnetic moment per supercell M (μ_B) and band gap E_g (eV) for H_2 adsorbed on phosphorene-based systems. The negative value of the Bader charge indicates H_2 as the charge acceptor. The E_F inside the parenthesis is without H_2 adsorption

System	E_a	ΔQ	h	d	d_{H-H}	E_F	M	E_g
$P_{48}@H_2$	-0.03	-0.003	3.33	3.43	0.75	-2.92 (-2.92)	*0*	0.89 (0.89)
$P_{45}Co_1Sn_2@H_2$	-0.35	-0.008	1.62	1.72	0.81	-2.91 (-2.80)	6.0	No (No)
$P_{45}Co_2Sn_1@H_2$	-0.48	-0.003	165	1.73	0.81	-2.87 (-2.77)	3.0	0.41(No)
$P_{45}Co_3@H_2$	-0.65	-0.011	1.41	1.71	0.80	-2.99 (-2.88)	6.0	0.21(0.20)

pristine phosphorene is non-magnetic in the ground states, however, when dopants are introduced, it may become magnetic. Our spin-polarized calculations reveal that all three doped models are magnetic in the ground state and exhibit an integer M. For instance, model-A has M = 6 μ_B, model-B has M = 3 μ_B, and model-C has M = 6 μ_B. In the model-A, the Co-atom has m = 1.98 μ_B, and each Sn-atom has m=-0.3 μ_B, which means coupling between Co and Sn-atoms is antiferromagnetic (AFM), and two Sn-atoms have ferromagnetic (FM) coupling, and the material is said to have a FM coupling. In addition, the P-atoms connected to Co/Sn-atoms carry a negligible moment. For model-B, one Co-atom has m= -1.51 μ_B and the other one has m = 1.87 μ_B, and Sn-atom has a tiny moment of m=-0.01 μ_B, confirming an overall ferrimagnetic (FIM) coupling in the material. In model-C, all the three doped Co-atoms have parallel moments, with one Co-atom carrying a moment of m = 1.3 μ_B, and the other ones having a moment of m = 2.1 μ_B. Thus, model-C has FM coupling in the ground state.

The electronic properties are investigated using electronic band structure (Fig. 4) and density of states (DOS) plots (Fig. 5). In Fig. 3(b-d), the black (red) lines represent the majority (minority) electronic states. We find that upon doping of Co/Sn-atoms the electronic structure of phosphorene has remarkably changed. For example, model-A and model-B have metallic characters, whereas model-B still exhibits semiconducting features but with a much-reduced band gap (E_g=0.2 eV). The DOS plots can help in understanding the underlying mechanism for change in the electronic properties of phosphorene. According to Fig. 4b, the mid-gap states that vanish the band gap belong to Co-atom with a major contribution, while P/Sn-atoms have a small contribution. Further analysis of ODOS (Fig. 5c/d) shows that the states emerging at the Fermi level (E_F) originate from P-2p, Co-p, and Sn-d orbital. The overlap of energy

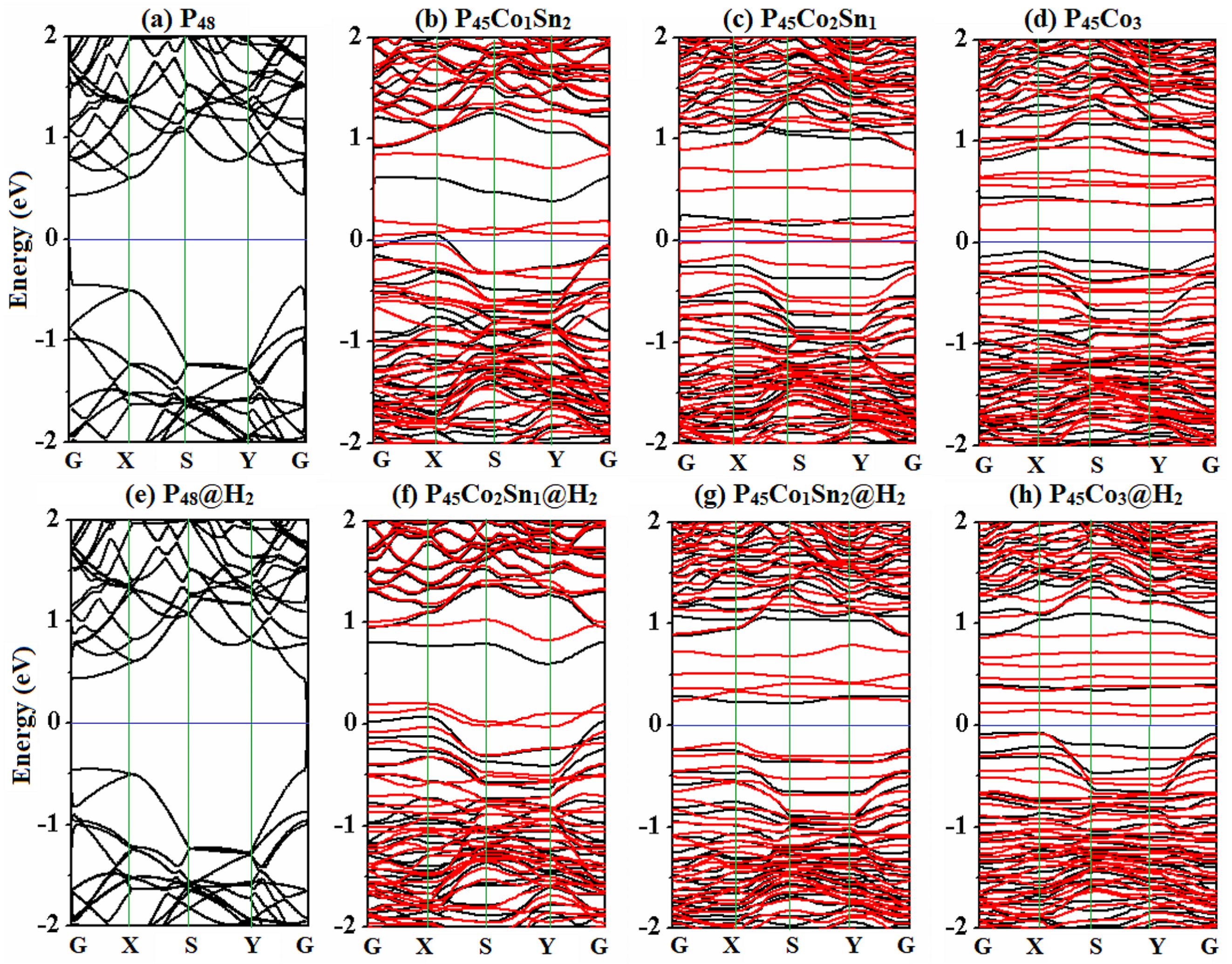

Fig. 4 Electronic band structure of (**a**) P_{48}, (**b**) $P_{45}Co_1Sn_2$, (**c**) $P_{45}Co_2Sn_1$, (**d**) $P_{45}Co_3$ without and with H_2 shown in (**e**), (**f**), (**g**) and (**h**).

states below E_F favors strong hybridization between host P-atom and dopants to form covalent bonds. In model-B, the energy states at E_F belong to P-2p, Co-p/d, and Sn-p/d orbital, which transform the band structure of the material to metallic. For model-C, the valence band edge is formed by both P and Co atoms, whereas the conduction band edge is mainly constructed by Co-atoms, and ODOS plots show that band edges have a mixed character of P-2p and Co-p/d states.

3.5 H_2 on phosphorene

In the following section, we discuss the effect of Co/Sn doping on the adsorption of H_2 on phosphorene. To estimate the effect of doping on adsorption strength, we first investigated H_2 adsorption on un-doped phosphorene, and then compared the adsorption parameters with those obtained with doped systems. In phosphorene, we considered some high symmetric adsorption sites such as top (T), hollow (H), bridge-1 (B1), and bridge-2 (B2), shown in supplementary information (Figure SI-1). Besides, we have also considered two landing orientations of the molecule, horizontal and vertical. In horizontal orientation, the H-H bond is parallel to the xy-plane of the phosphorene structure, and in vertical orientation, the H-H bond is perpendicular to xy-plane of the phosphorene. In this way, we obtain eight adsorption configurations (AC). To determine the energetically favorable AC each configuration is relaxed with spin-polarized calculations by allowing all atoms (of molecule and adsorbent) to move freely in all directions. After calculations, it was found that B2 site has the lowest total energy, therefore it is marked as the most stable AC. Afterward, the desired adsorption parameters (adsorption energy, charge transfer, adsorption height, etc.) are calculated for this stable AC, listed in Table 1. The relaxed AC at B2 is presented in Fig. 6a. It is noticed that H_2 molecule moves away from the surface and does not interact chemically. The adsorption parameters show that H_2 is physically adsorbed as evidenced

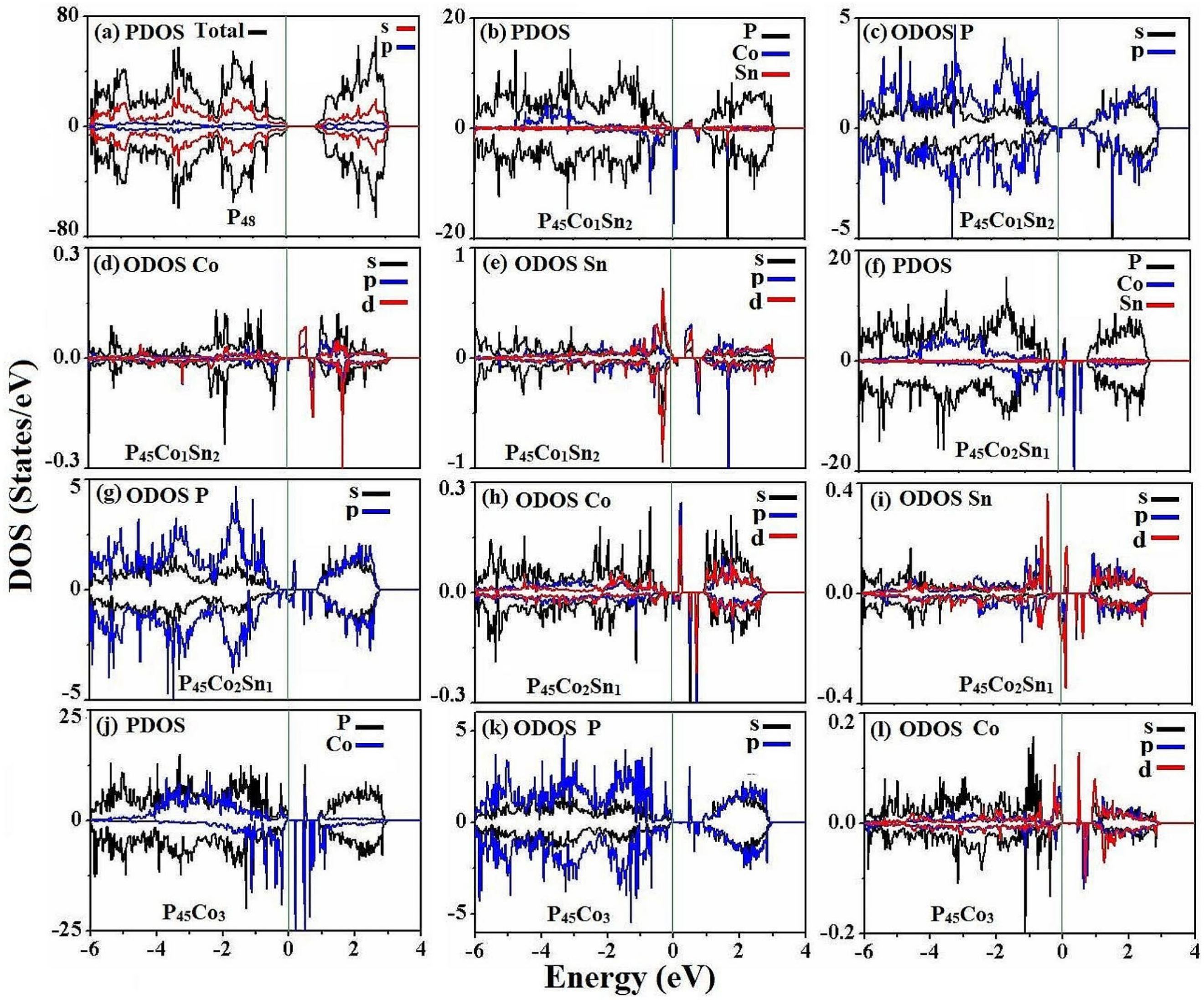

Fig. 5 Electronic density of states (DOS) plots for (**a**) P_{48}, (**b-e**) $P_{45}Co_1Sn_2$, (**f-i**) $P_{45}Co_2Sn_1$, (**j-l**) $P_{45}Co_3$

by very small adsorption energy (E_a) of -0.03 eV, and a large adsorption height (h) of 3.33 Å. The band structure of H_2 adsorbed on phosphorene ($P_{48}@H_2$) presented in Fig. 3(e) is exactly like that of phosphorene without H_2, confirming that the molecule did not alter the electronic properties of phosphorene. In short, pristine phosphorene cannot be used for the capture or detection of H_2.

3.6 H_2 on doped phosphorene

The adsorption of H_2 on the doped systems is examined at various doping sites including the top of Co-atom, the top of Sn-atom, and between Co and Sn-atoms. We explain the adsorption profile on each doped system one by one. Firstly, in model-A (Fig. 6b), the molecule is preferably adsorbed on the Co-atom. For this site, the calculated values of adsorption parameters (E_a, ΔQ, h, d_{min}, etc.) are listed in the table. The calculated values show that the adsorption of the molecule on this site is exothermic as the adsorption energy is negative. In addition, the molecule forms chemical bonds with Co-atom, evidenced by the small values of h = 1.62 Å and d_{min}=1.72 Å. The H-H bond length is slightly increased after adsorption from the initial value of 0.75 Å to 0.81 Å. As H_2 molecule interacts with the adsorbent only via Co-atom, and Co and H-atoms have different electronegativity, therefore one may expect an exchange of charge (ΔQ) between two adsorbent and adsorbate. Our results indicate a small value of ΔQ=-0.008e, and its negative sign indicates the charge is transferred from the adsorbent to the molecule. Thus, the H_2 molecule acts as a charge accepter when adsorbed on model-A. The adsorption of H_2 slightly shifts the position of the Fermi level towards lower energy from the actual value of -2.80 eV. Interestingly, such adsorption did not alter the electronic band gap and magnetic moment

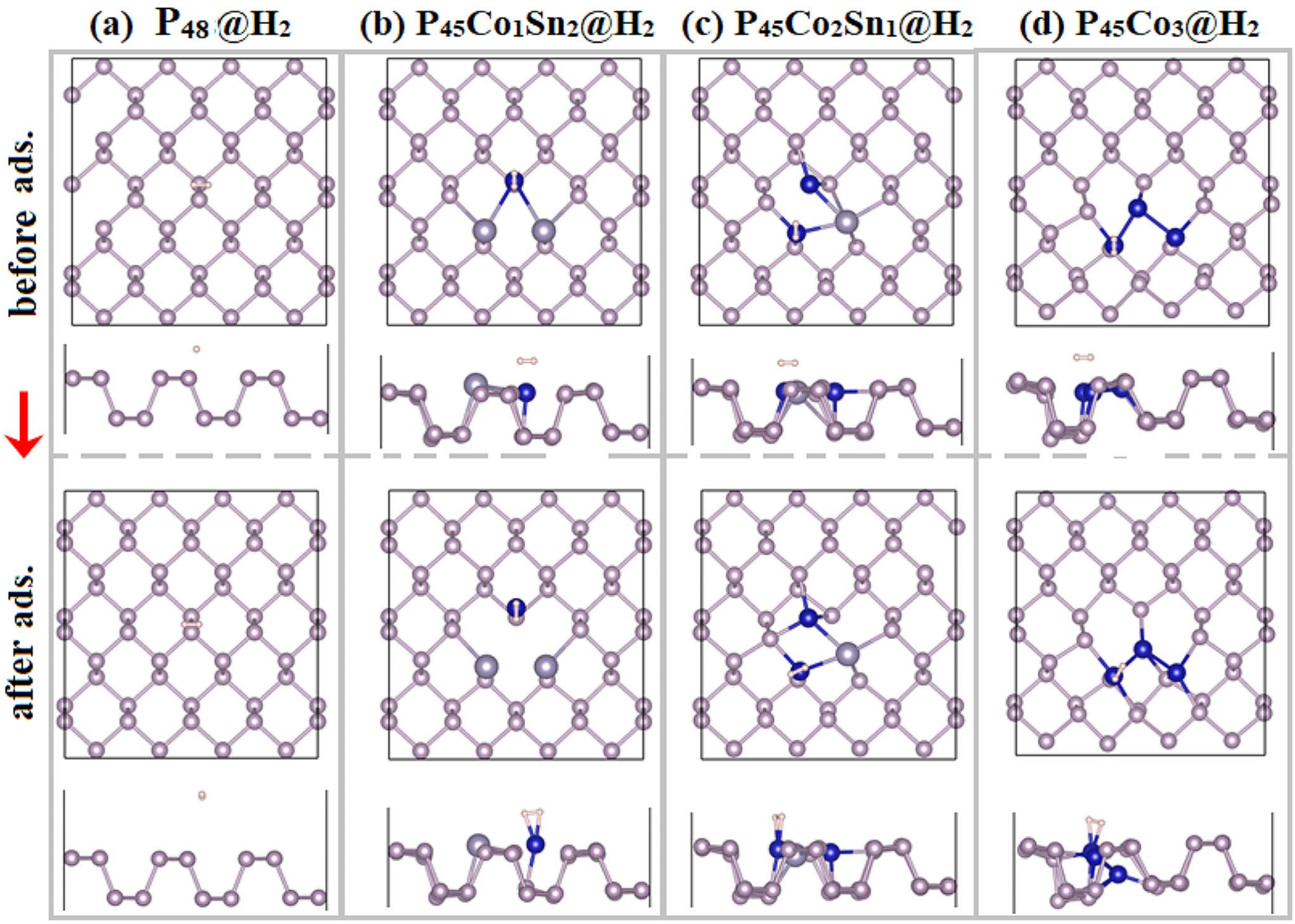

Fig. 6 Initial (upper-panel) and final (lower-panel) configuration of H_2 adsorbed on (**a**) P_{48}, (**b**) $P_{45}Co_1Sn_2$, (**c**) $P_{45}Co_2Sn_1$, (**d**) $P_{45}Co_3$

of the adsorbent. In model-B, the most favorable AC is obtained when the molecule is adsorbed on Co-atom. The adsorption parameters listed in the table, do not much differ from those of model-A. Therefore, we predict that the molecule is chemically adsorbed on model-B. For model-C, again the most favorable AC is obtained on the top of the Co-atom. However, the adsorption strength is increased as seen from the value of E_a=-0.65 eV. For practical purposes, very large or small adsorption energy is considered unfavorable for reversible sensing. In our case, the adsorption energy is moderate, and suitable for capturing H_2 molecules for energy storage applications.

3.7 Mechanism for H_2 adsorption on doped phosphorenee

To deeply explore the underlying mechanism behind the observed chemisorption of H_2 on doped phosphorene, electronic density of states and charge density difference (CDD) plots are provided in Figs. 7 and 8, respectively. We find that in all adsorption cases, VBE and CBE states of the $P_{45}Co_1Sn_2@H_2$ system are mainly formed by the adsorbent atoms, while ODOS of Co and H reveal that Co-d and H-s orbital have a clear spin-polarization as the majority and minority states near the Fermi level are asymmetric over the given energy region. The presence of Co-d and H-s states just below and at the Fermi level is an indication of the hybridization of these orbitals, which causes binding between two atoms. Thus, the H_2 molecule interacts with the adsorbent via s-d interaction and facilitates the exchange of charge between two species.

The CDD plots can help in understanding the exchange of charge between adsorbent and adsorbate. When an adsorbent is chemically adsorbed on the surface of an adsorbent, due to the exchange of charge, the distribution of charge is deformed particularly at the site where adsorption occurs. This redistribution of charge can be visualized in different color regions. In Fig. 8, two types of regions can be differentiated, yellow ones and cyan ones. The yellow regions located around doped atoms represent the depletion of charge while cyan regions show charge accumulation, this is because Co-atoms donate charge to H-atoms of H_2 molecule when come in close interaction. This exchange of charge is also responsible for a considerable binding between

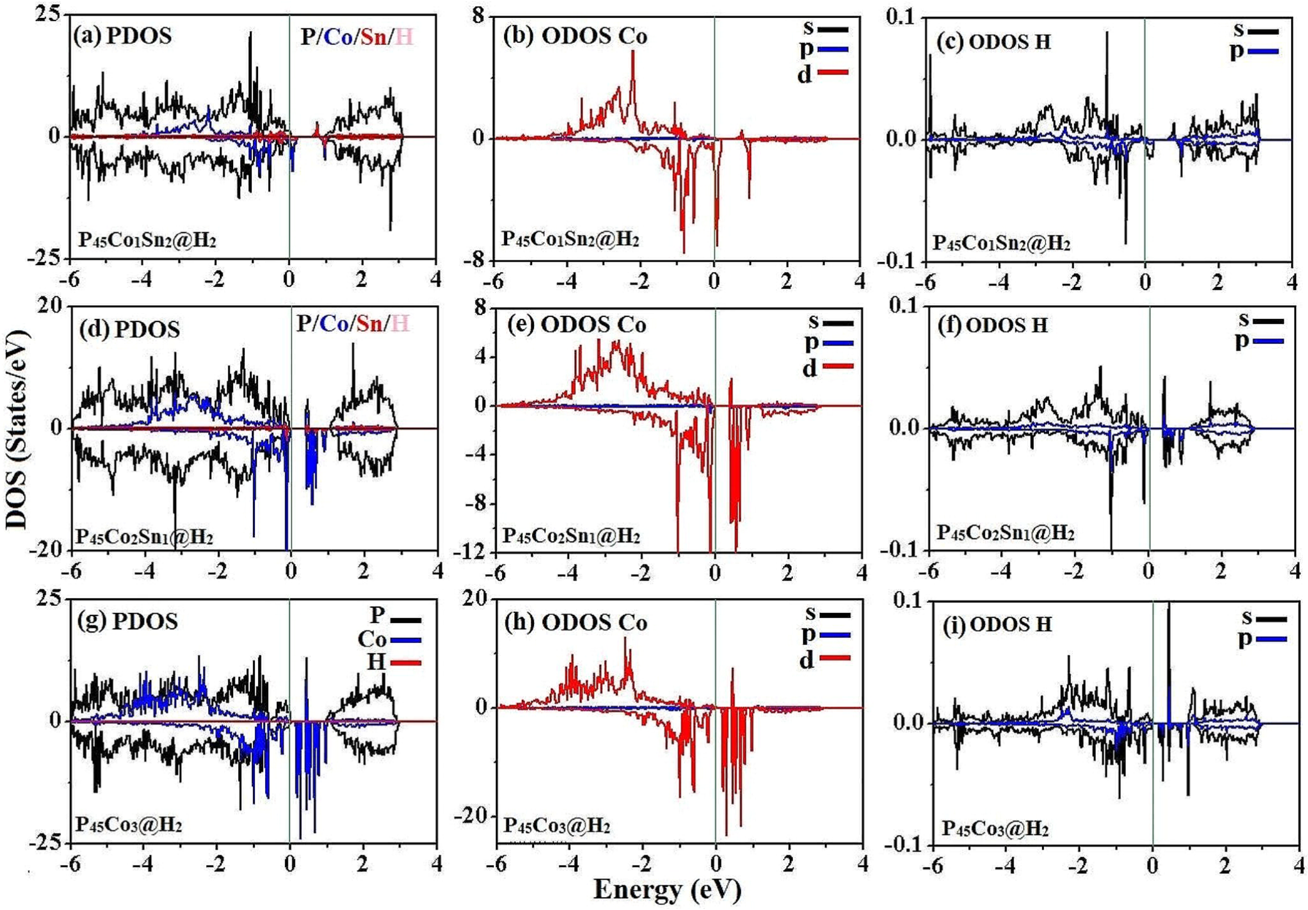

Fig. 7 Electronic density of states for H_2 molecule adsorbed on (**a-c**) $P_{45}Co_1Sn_2$, (**d-f**) $P_{45}Co_2Sn_1$, (**g-i**) $P_{45}Co_3$

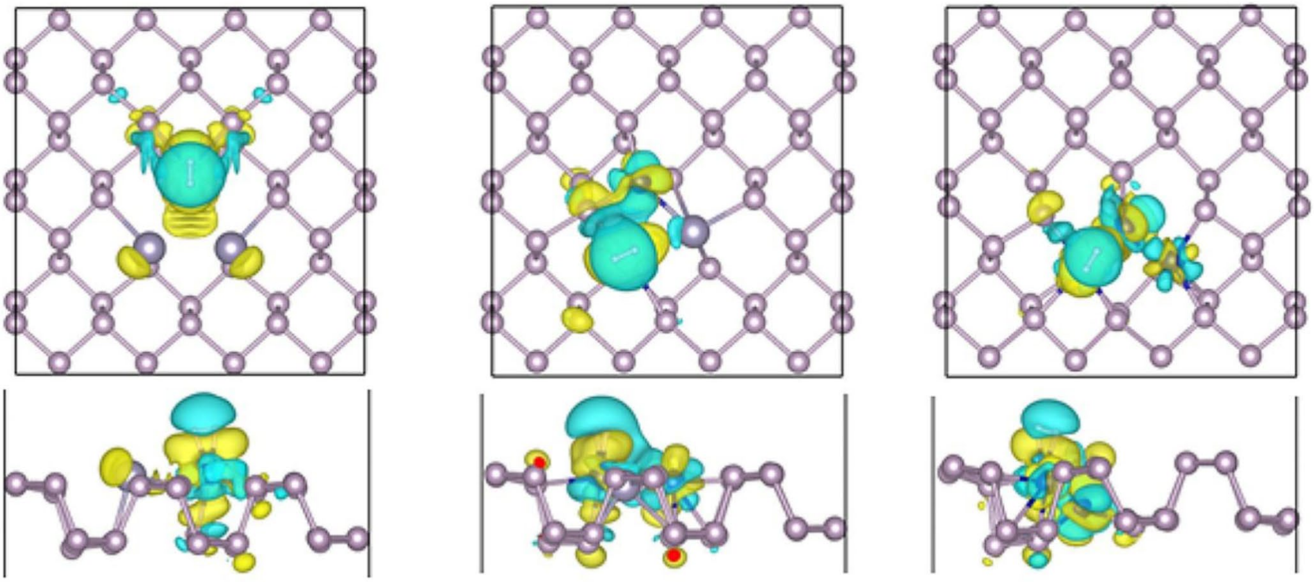

(a) $P_{45}Co_1Sn_2@H_2$ (b) $P_{45}Co_2Sn_1@H_2$ (c) $P_{45}Co_3@H_2$

Fig. 8 Charge density difference (CDD) for H_2 molecule adsorbed on (**a**) $P_{45}Co_1Sn_2$, (**b**) $P_{45}Co_2Sn_1$, (**c**) $P_{45}Co_3$

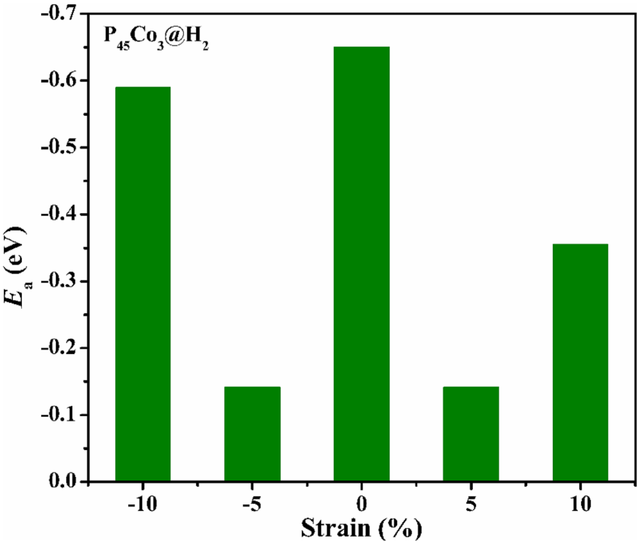

Fig. 9 Variation of adsorption energy with strain for H_2 adsorbed on $P_{45}Co_3$.

adsorbent and H_2 molecule. In short, we conclude that, unlike pristine phosphorene where H_2 is weakly adsorbed, the adsorption strength is remarkably enhanced when Co and Sn-atoms are simultaneously doped into phosphorene, resulting in the chemisorption of H_2 molecule.

3.8 Strain effect on adsorption

Strain is extensively used for tuning the adsorption ability of 2D materials [40, 41]. To explore its effect, the adsorption of H_2 is investigated on various strained systems of Co-doped phosphorene. The resulting adsorption energy at the biaxial strain value of -10%, -5%, 0%, 5%, and 10% is plotted, shown in Fig. 9. The negative (positive) strain indicates compression (elongation). It is found that E_a decreases for both positive and negative strains, indicating that interaction between the adsorbent and H_2 is sensitive to the interatomic bond lengths. It is useful to mention that strain has a direct impact on the interatomic bond lengths: for compressive strain, the interatomic bond lengths tend to decrease and vice versa. The change in bond lengths affects the interaction between two reactants.

3.9 Adsorption of multiple H_2

In the adsorption of multiple H_2 molecules, the average adsorption (E_{av}) was calculated as defined in ref. 7.

$$E_{av} = \frac{E(nH_2 + P_{45}Co_xSn_y) - E\left(P_{45}Co_xSn_y\right) - nE\left(H_2\right)}{n} \tag{2}$$

where the first, second, and third terms indicate the total energy of the product, absorbent, and adsorbate. The integer n represents the number of H_2 molecules loaded on the surface of the adsorbent. The adsorption capacity or the ability to capture the maximum number of molecules is an important factor in sensing. To estimate how many molecules can be adsorbed, we calculated the average adsorption energy (E_{av}). The E_{av} is defined as the adsorption energy ($E_{av}=E_a/n$) per number of molecules (n) adsorbed. The resulting data is plotted in Fig. 10 and the final configuration of seven H_2 molecules is shown in Figure SI-2. It is noticed that E_{av} decreases with n value. For $n=7$, the E_{av} is about -0.2 eV for $P_{45}Co_3$ and $P_{45}Co_1Sn_2$. This might be due to repulsion among neighboring H_2 molecules and/or due to the presence of a limited number of active sites to capture H_2.

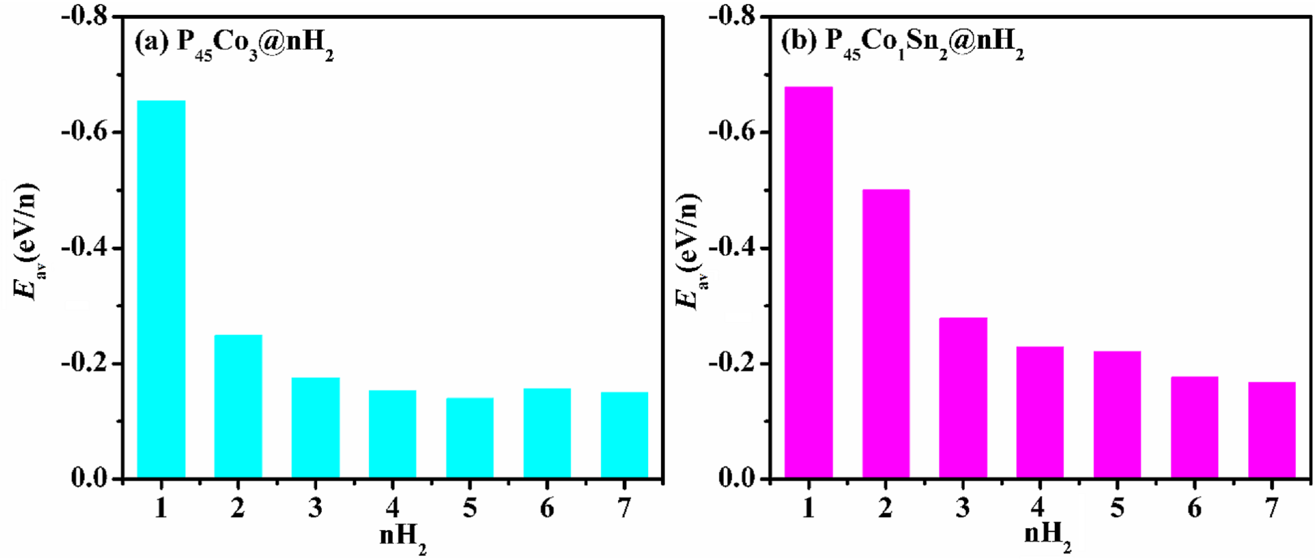

Fig. 10 Variation of average adsorption energy (E_{av}) with the number of H_2 molecules loading on (**a**) $P_{45}Co_3$, and (**b**) $P_{45}Co_1Sn_2$

4 Conclusion

In this work, the effect of Co/Sn co-doping on the electronic, magnetic, and adsorption properties (for H_2 capture) of monolayer phosphorene was investigated using first-principles calculations. Unlike pristine phosphorene (P_{48}), the co-doped phosphorene ($P_{45}Co_xSn_y$) can exhibit ferrimagnetic (FIM) or ferromagnetic (FM) coupling in the ground state. The doped structures exhibit integral magnetic moments, mainly contributed by the Co-atoms. The $P_{45}Co_1Sn_2$ and $P_{45}Co_2Sn_1$ structures show metallic band structure, while $P_{45}Co_3$ becomes a small band gap (E_g) semiconductor (E_g =0.2 eV). The adsorption of H_2 molecule was investigated on un-doped and co-doped phosphorene. It was found that H_2 molecule is weakly adsorbed on un-doped phosphorene, whereas moderate adsorption was observed for co-doped systems. The adsorption energy (E_a) was found to be -0.03, -0.35, -0.48, and − 0.65 eV, respectively for P_{48}, $P_{45}Co_1Sn_2$, and $P_{45}Co_2Sn_1$ and $P_{45}Co_3$, respectively. The reported E_a values for co-doped phosphorene are well close to the ideal E_a of -0.5 eV, suitable for reversible adsorption. The DOS plots confirmed that the observed adsorption is due to the overlap of the s-orbital of the H-atom and the d-orbital of the Co-atom. The Bader charge analysis showed that the H_2 molecule acts as a charge acceptor and doped phosphorene as a charge donor. These findings show that co-doped phosphorene can be used for spin-based nanodevices and hydrogen capture for energy storage applications.

Supplementary Information The online version contains supplementary material available at https://doi.org/10.1007/s10450-024-00516-0.

Acknowledgements This work was funded by the Deanship of Graduate Studies and Scientific Research at Jouf University under grant No (DSR2023-03-02052).

Author contributions Conceptualization, A.M., A.A. and M.A.; methodology, A.M., M.A., M.M., and A.L.; software, A.M., M.M., and M.A.; validation, A.M., A.A., MA and A.L.; formal analysis, A.M., A.A. and M.A.; investigation, A.A. and A.L.; data curation, A.M., M.M., A.A. and M.A.; writing original draft preparation, A.M.; writing review and editing, A.M., M.A.; visualization, A.A., M.M., M.A. and A.L.; supervision, A.M.; project administration, A.M.; funding acquisition, A.M. All authors have read and agreed to the published version of the manuscript.

Data availability No datasets were generated or analysed during the current study.

Declarations

Ethical approval Not applicable.

Competing interests The authors declare no competing interests.

References

1. Le, T.T., Sharma, P., Bora, B.J., Tran, V.D., Truong, T.H., Le, H.C., et al.: Fueling the future: A comprehensive review of hydrogen energy systems and their challenges. Int. J. Hydrog. Energy. **54**, 791–816 (2024)
2. Nikolaidis, P., Poullikkas, A.: A comparative overview of hydrogen production processes. Renew. Sustain. Energy Rev. **67**, 597–611 (2017)
3. Pasquini, L.: Design of Nanomaterials for Hydrogen Storage. 13, 3503. (2020)
4. Ian Jason, J., Pal, Y., Anees, P., Lee, H., Kaewmaraya, T., Hussain, T., et al.: Defects induced metallized boron hydride monolayers as high-performance hydrogen storage architecture. Int. J. Hydrog. Energy. **50**, 455–463 (2024)
5. Kumar, N., Sharma, M., Pandey, R.: Tit, N. Borophene/graphene heterostructure for effective hydrogen storage with facile dehydrogenation. Int. J. Hydrog. Energy. **70**, 510–521 (2024)
6. Kaur, S.P., Hussain, T., Kaewmaraya, T., Kumar, T.J.D.: Reversible hydrogen storage tendency of light-metal (Li/Na/K) decorated carbon nitride (C_9N_4) monolayer. Int. J. Hydrog. Energy. **48**, 26301–26313 (2023)
7. Yuan, L., Kang, L., Chen, Y., Wang, D., Gong, J., Wang, C., et al.: Hydrogen storage capacity on Ti-decorated porous graphene: First-principles investigation. Appl. Surf. Sci. **434**, 843–849 (2018)
8. Novoselov, K.S., Geim, A.K., Morozov, S.V., Jiang, D., Zhang, Y., Dubonos, S.V., et al.: Electric field effect in atomically thin carbon films. Science. **306**, 666–669 (2004)
9. Fathzadeh, M., Fahrvandi, H., Nadimi, E.: Electronic properties of graphene-ZnO interface: A density functional theory investigation. Nanotechnology. **31**, 025710 (2019)
10. Cahangirov, S., Topsakal, M., Akturk, E., Sahin, H., Ciraci, S.: Two- and one-dimensional honeycomb structures of silicon and germanium. Phys. Rev. Lett. **102**, 236804 (2009)
11. Şahin, H., Cahangirov, S., Topsakal, M., Bekaroglu, E., Akturk, E., Senger, R.T., et al.: Monolayer honeycomb structures of group-IV elements and III-V binary compounds: First-principles calculations. Phys. Rev. B. **80**, 155453 (2009)
12. Jin, C., Lin, F., Suenaga, K., Iijima, S.: Fabrication of a freestanding boron nitride single layer and its defect assignments. Phys. Rev. Lett. **102**, 195505 (2009)
13. Chhowalla, M., Shin, H.S., Eda, G., Li, L.-J., Loh, K.P., Zhang, H.: The chemistry of two-dimensional layered transition metal dichalcogenide nanosheets. Nat. Chem. **5**, 263–275 (2013)
14. Khazaei, M., Arai, M., Sasaki, T., Chung, C.-Y., Venkataramanan, N.S., Estili, M., et al.: Novel Electronic and Magnetic Properties of Two-Dimensional Transition Metal Carbides and Nitrides. Adv. Funct. Mater. **23**, 2185–2192 (2013)
15. Gao, G., Ding, G., Li, J., Yao, K., Wu, M., Qian, M.: Monolayer MXenes: Promising half-metals and spin gapless semiconductors. Nanoscale. **8**, 8986–8994 (2016)
16. Zha, X.-H., Yin, J., Zhou, Y., Huang, Q., Luo, K., Lang, J., et al.: Intrinsic Structural, Electrical, Thermal, and Mechanical properties of the Promising Conductor Mo2C MXene. J. Phys. Chem. C. **120**, 15082–15088 (2016)
17. Yorulmaz, U., Ozden, A., Perkgoz, N.K., Ay, F., Sevik, C.: Vibrational and mechanical properties of single layer MXene structures: A first-principles investigation. Nanotechnology. **27**, 335702 (2016)
18. Li, X., Mullen, J.T., Jin, Z., Borysenko, K.M., Buongiorno Nardelli, M., Kim, K.W.: Intrinsic electrical transport properties of monolayer silicene and MoS_2 from first principles. Phys. Rev. B. **87**, 115418 (2013)

19. Babar, V., Sharma, S., Schwingenschlögl, U.: New Paradigm for Gas sensing by two-dimensional materials. J. Phys. Chem. C. **123**, 13104–13109 (2019)
20. Liu, H., Neal, A.T., Zhu, Z., Luo, Z., Xu, X., Tománek, D., et al.: Phosphorene: An unexplored 2D Semiconductor with a high hole mobility. ACS Nano. **8**, 4033–4041 (2014)
21. Guo, G.-C., Wei, X.-L., Wang, D., Luo, Y., Liu, L.-M.: Pristine and defect-containing phosphorene as promising anode materials for rechargeable Li batteries. J. Mater. Chem. A. **3**, 11246–11252 (2015)
22. Zhang, S., Yan, Z., Li, Y., Chen, Z., Zeng, H.: Atomically thin arsenene and antimonene: Semimetal-semiconductor and indirect-direct band-gap transitions. Angew Chem. Int. Ed. Engl. **54**, 3112–3115 (2015)
23. Ji, J., Song, X., Liu, J., Yan, Z., Huo, C., Zhang, S., et al.: Two-dimensional antimonene single crystals grown by Van Der Waals epitaxy. Nat. Commun. **7**, 13352 (2016)
24. Shah, J., Wang, W., Sohail, H.M., Uhrberg, R.I.G.: Experimental evidence of monolayer arsenene: An exotic 2D semiconducting material. 2D materials. **7**, 025013. (2020)
25. Kou, L., Chen, C., Smith, S.C., Phosphorene: Fabrication, Properties, and applications. J. Phys. Chem. Lett. **6**, 2794–2805 (2015)
26. Ares, P., Palacios, J.J., Abellán, G., Gómez-Herrero, J., Zamora, F.: Recent progress on Antimonene: A New Bidimensional Material. Adv. Mater. **30**, 1703771 (2018)
27. Srivastava, P., Hembram, K.P.S.S., Mizuseki, H., Lee, K.-R., Han, S.S., Kim, S.: Tuning the electronic and Magnetic Properties of Phosphorene by vacancies and Adatoms. J. Phys. Chem. C. **119**, 6530–6538 (2015)
28. Liu, B., Bai, L., Korznikova, E.A., Dmitriev, S.V., Law, A.W.-K., Zhou, K.: Thermal conductivity and Tensile Response of Phosphorene nanosheets with Vacancy defects. J. Phys. Chem. C. **121**, 13876–13887 (2017)
29. Hu, W., Yang, J.: Defects in Phosphorene. J. Phys. Chem. C. **119**, 20474–20480 (2015)
30. Garara, M., Benzidi, H., Lakhal, M., Louilidi, M., Ez-Zahraouy, H., El Kenz, A., et al.: Phosphorene: A promising candidate for H2 storage at room temperature. Int. J. Hydrog. Energy. **44**, 24829–24838 (2019)
31. Yu, Z., Lei, S., Wan, N., Luan, S., Shen, H., Yu, H.: Effect of metal adatoms on hydrogen adsorption properties of phosphorene. Mater. Res. Express. **4**, 045503 (2017)
32. Kresse, G., Furthmüller, J.: Efficient iterative schemes for ab initio total-energy calculations using a plane-wave basis set. Phys. Rev. B. **54**, 11169–11186 (1996)
33. Perdew, J.P., Burke, K., Ernzerhof, M.: Generalized gradient approximation made simple. Phys. Rev. Lett. **77**, 3865–3868 (1996)
34. Liu, B.-L., Wang, Y.-C., Liu, Y., Xu, Y.-J., Chen, X., Song, H.-Z., et al.: Comparative study of first-principles approaches for effective Coulomb interaction strength Ueff between localized f-electrons: Lanthanide metals as an example. J. Chem. Phys. **158**, 084108 (2023)
35. Lin, C.-Y., Zhang, L., Zhao, Z., Xia, Z.: Design principles for Covalent Organic frameworks as efficient electrocatalysts in Clean Energy Conversion and Green Oxidizer production. Adv. Mater. **29**, 1606635 (2017)
36. Tang, Y., Zhou, W., Hu, C., Pan, J., Ouyang, F.: Electronic and magnetic properties of phosphorene tuned by cl and metallic atom co-doping. Phys. Chem. Chem. Phys. **21**, 18551–18558 (2019)
37. Ullah, S., Denis, P.A., Sato, F.: Triple-doped monolayer graphene with Boron, Nitrogen, Aluminum, Silicon, Phosphorus, and Sulfur. ChemPhysChem. **18**, 1864–1873 (2017)
38. Denis, P.A.: Mono and dual doped monolayer graphene with aluminum, silicon, phosphorus and sulfur. Comput. Theor. Chem. **1097**, 40–47 (2016)
39. Mushtaq, M., Godara, S., Khenata, R., Usman Hameed, M.: Effect of Si, be, Al, N and S dual doping on arsenene: First-principles insights. RSC Adv. **11**, 25217–25227 (2021)
40. Liu, Q., Zhao, W., Ao, Z., An, T.: Photo-piezoelectric synergistic degradation of typical volatile organic compounds on $BaTiO_3$. Chin. Chem. Lett. **33**, 410–414 (2022)
41. Zhu, Y., Zhao, W., Jing, B., Zhou, J., Cai, B., Li, D., et al.: Density functional theory calculations on 2H-MoS_2 monolayer for HCHO degradation: Piezoelectric-photocatalytic synergy. Chin. Chem. Lett. **34**, 107816 (2023)